Cloud Characterization in the S/MWIR Using a Linear Least Squares Algorithm*

Jennifer C. Davis Jerry X. Tull James J. Lisowski
SciTec, Inc.
100 Wall Street
Princeton, NJ 08540
(609) 921-3892
jend@scitec.com jtull@scitec.com jiml@scitec.com
and
Capt. Todd Caldwell
NAIC/DXDI
4180 Watson Way
Wright-Patterson AFB, OH 45433
(937)257-2575
wtc52@naic.wpafb.af.mil

Abstract – In remote sensing applications, the problem of cloud obscuration is widespread. Characterization of these clouds, however, can help to alleviate their effects on scene feature discrimination. Thus, algorithms useful in distinguishing cloudy from clear pixels, and further, in approximating the temperature, particle characteristics, and altitude of the clouds, can improve the quality of many remote sensing missions. To this end, we present here further developments concerning the Cloud Detection and Identification (CloudDI) algorithm, which was first presented in 1998 at the IEEE Aerospace Conference. We concentrate upon using CloudDI to process spectral data in the short and midwave infrared (S/MWIR), and compare our cloud characterization results using multiple bands (e.g., 49 channels) and reduced spectral resolution cases (e.g. 5-8 bands).

First, we describe our studies concerning the detection and typing of multiple cloud layers using ARES (Airborne Remote Earth Sensing) flight data. We show that these multiple cloud layers can, in some cases, be detected using suitable CloudDI templates. Particular attention is given to modeling the attenuation of the radiance from low-lying clouds by a thin cover of high-altitude cirrus clouds. Although this type of discrimination necessitates the presence of multiple cloud templates in the CloudDI matrix, we show that as few as two cloud templates can be used (in addition to an in-scene terrain pixel) to roughly discriminate between ice and water clouds and between cloud and terrain pixels. We also propose a method for directly determining cloud top temperature from midwave infrared (MWIR) bands, using a modified CloudDI routine that removes the reflected solar component from the measured radiance. This temperature information can then be used to infer cloud altitudes.

Another important consideration in algorithm development is the speed at which acceptably accurate results can be obtained - particularly for real-time weather characterization efforts. Often, the speed-accuracy trade-off shifts depending upon the application. Here, we present our studies concerning the trade-off between the computation time and information value contained in various implementations of CloudDI. In these experiments, we examine the effects of adding and subtracting spectral points, and of replacing the constrained version of the CloudDI algorithm with a (non-iterative) unconstrained implementation.

Essentially, in the CloudDI algorithm, the scene pixel spectra are compared with the spectral signature predictions of a variety of clouds and selected terrain features generated with spectral radiance models, using a linear least squares approach. An important part of the CloudDI method, then, is the calculation of these cloud and terrain "templates". In order to optimize this process, we studied three spectral radiance modeling programs - MODTRAN, MOSART and HYPEX - and will delineate some of the differences we have found between them (e.g., cloud model resources, run times, multiple scattering algorithms).

TABLE OF CONTENTS

* 7803-5846-5/00/$10.00 © 2000 IEEE

1. INTRODUCTION

Remote sensing missions are frequently plagued by clouds, which distort or completely obscure target features. Characteristics such as the altitude, particle size, and ice/water composition of these clouds can be ascertained, however, using a variety of spectral methods. This type of information can be critical, for example, to pilots making fly/no fly decisions, or to meteorolgists in compiling their weather forcasts. Furthermore, surface temperatures can be ascertained [insert Burke ref. (presentation)] and targets can sometimes be reconstructed via Monte Carlo-based methods such as those implemented by Brower [1,2] at Sandia National Labs (SNL), using such cloud data. There are currently a variety of techniques for characterizing clouds ranging from simple threshold tests, in which radiance values from a single spectral band are exploited, to complicated iterative algorithms for calculating atmospheric sounding profiles (based upon data from a multitude of spectral bands).

The determination of which of these cloud-characterization tests to use for a given application is based primarily upon the spectral channels available for data collection and the nature of the information required. For instance, in a report prepared by Phillips Laboratory at Hanscom AFB [3], a number of relatively simple threshold and multispectral ratio tests are described for operation using DMSP/OLS, NOAA/AVHRR, GOES/VAS, METEOSAT/VISSR, and GMS/VISSR sensor data. All of these sensors have channels in both the visible (VIS) and long wave infrared (LWIR) spectral regions. Here, however, we are concerned with radiance data only in the short- and mid-wave infrared (S/MWIR). In the S/MWIR, assessing the spectral characteristics (i.e., the respective contributions of direct IR emission and reflection of solar radiation) of an object is not always as straightforward as in the LWIR. This is easily seen upon inspection of Figure 1, in which a daytime solar radiance curve (the direct solar component calculated by MODTRAN for an albedo of 0.1) is plotted along with thermal radiance curves at 200 K and 300 K – the approximate range of terrestrial temperatures. In the visible region, solar radiation (reflection and scattering by the object and atmospheric path) dominates whereas in the LWIR, the (self-emitted) thermal radiation values exceed the solar values by orders of magnitude.

In the transmission window MWIR (approximately 3.0 to 4.8 µm, not including the 4.3 µm CO_2 band), solar radiation and blackbody radiation are often of the same order of magnitude. This usually makes distinguishing the object's self-emission from the scattered or reflected solar radiation difficult. The MWIR itself, however, may be divided into two distinct subregions for the purpose of choosing spectral bands to use in remote temperature calculations. In reference [4], for example, the authors divide the MWIR into a 2.7 to 4.2 µm subregion and a 4.6 to 4.9 µm subregion. In the 2.7 to 4.2 µm subregion, the reflected and self-emitted radiation values are typically of the same order of magnitude in the daytime. In the 4.6 to 4.9 µm band, on the other hand, the thermal radiation dominates the reflected solar radiation when the viewing geometry is non-specular. Since this is the case, the object's radiance may be used to approximate its temperature (after subtracting the path radiance as calculated by a program such as MODTRAN or MOSART, dividing by the path transmission, and comparing to Planck blackbody curves). We therefore propose using data from the ARES channels in the 4.6 to 4.9 µm spectral region to approximate cloud top temperatures. The authors in reference [4] were able to remotely calculate temperatures from MWIR data across horizontal paths ranging from 30 m to 10 km using this method.

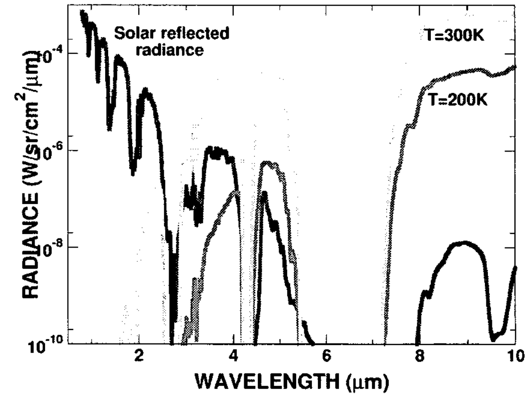

Figure 1. Typical contribution of thermal and solar radiation to total radiance

Significantly, they found that the temperature calculations using data from the 4.6- to 4.9-µm band were of comparable accuracy to similar calculations using data from the (more standard) 10.5- to 12.5-µm band. It should be noted that the measurements in [4], were taken over a horizontal path. Therefore, the reflected solar radiance measured in these experiments is less significant than that measured over a down-looking path (i.e., in ARES missions). Nevertheless, it is likely that radiance measurements in the 4.6 to 4.9 µm spectral region may similarly be used to deduce the approximate temperature of clouds from MWIR remote sensing mission data as we propose.

To date, several cloud characterization studies using a variety of methods [5,6,7,8,9] have been implemented upon ARES (Airborne Remote Earth Sensing) S/MWIR data. These include CloudDI [5,6], SAALT (Spectral Angle Automatic cLuster rouTine - an unsupervised clustering method described in detail in ref. [7]), a supervised clustering technique and atmospheric water vapor retrieval method (which makes use of data from 18 ARES channels in the 4.8 to 6.0 µm spectral region) [8], and a method for cirrus cloud characterization that is based upon data from the 3.7- and 5.1-5.3 µm ARES channels[9].

In references [5] and [6], we presented work done on the CloudDI (linear least squares) algorithm. In [5], 49 ARES channels with high SNR were employed to analyze single scene pixels and in [6], reduced spectral resolution (7 bands) was compared with full resolution test cases. Furthermore, test cases in which visible bands were added to the algorithm using synthetic scene data (SSGM) were presented. In this study, it was found that CloudDI was somewhat more accurate in predicting the presence of the modeled clouds and the altitude of those clouds it found using the visible band data than in making the same predictions using the ARES data in the S/MWIR bands only. This difference may be a result of the quality of the templates used in the analysis of ARES data, however. We will discuss this issue further below.

Here, we present a continuation of our studies using the CloudDI algorithm. We focus our attention upon using only a few carefully selected short- and mid-wave IR bands and show that in most cases the reduced spectral resolution is usually adequate for cloud characterization. Furthermore, we present the results of our experiments in which we have accounted for the attenuation of the radiance from low-lying clouds by overhead thin cirrus clouds. We also propose the integration of a cloud top temperature-calculating algorithm into CloudDI, in which data from the MWIR bands are exploited. Finally, we compare the efficiency and accuracy of different versions of CloudDI in which we have subtracted bands (and templates), removed constraints from the linear least squares computation, and altered the method used for calculating the CloudDI templates.

2. SCENE DATA

The scene data used for these experiments originate from ARES remote sensing missions (see, for example, references [10,11,12, and 13]).

ARES scenes

For the ARES project, a NASA WB-57F aircraft hosted a Lockheed-Martin Palo-Alto Research Laboratory (LMPARL) dual-mode radiometer/imaging spectrometer in order to collect spatially- and spectrally-resolved images in the 2.2 to 6.4 µm region. The focal plane array (FPA) of this device contains 45 x 90 elements, and may be configured either as a 45 x 45 pixel staring radiometer or as a 45 x 75 pixel spectrometer. A variety of scene data for over thirty missions were collected under the aegis of the Space-Based Infrared System (SBIRS) Phenomenology Exploitation Program (PEP) in 1995 and 1996. These scenes contain an assortment of different cloud types, including altostratus, cumulus, and cirrus, and were collected over urban, suburban, rural, and marine backgrounds.

The data we exploit here were collected on 16 September, 1995 over Hanscom AFB, MA [14] employing two different modes of operation: semicircle stare and pushbroom trajectories. For the pushbroom trajectory tracks, the sensor was placed in a nadir staring orientation and the aircraft was flown along a straight path. Data were therefore collected in a single swath. In the semicircle trajectory tracks, the sensor was pointed at a spot 8 km above the ground station at Hanscom with a look zenith angle (LZA) of 70°. These trajectories are delineated in Figure 2. Of the seven data tracks, 1, 3, and 5 were collected in the pushbroom mode, and 2, 4, 6, and 7 were collected in the semicircle mode. In our previous CloudDI experiments, we found that the thin clouds that were characteristic of these scenes were difficult to detect in the nadir-viewed (pushbroom) tracks. In the 70° LZA collects, on the other hand, CloudDI easily detected the thin clouds. This difference is most likely due to the effective thickness of the clouds measured by the sensor in each respective case. In the 70° case, the path through the clouds is significantly longer than in the nadir case, thereby increasing the clouds' effective thickness. Here, we concentrate on nadir-viewed data from Track 1. Ground-based, RADAR data were collected contemporaneously to the Hanscom ARES missions on 16 September and are used to validate our results.

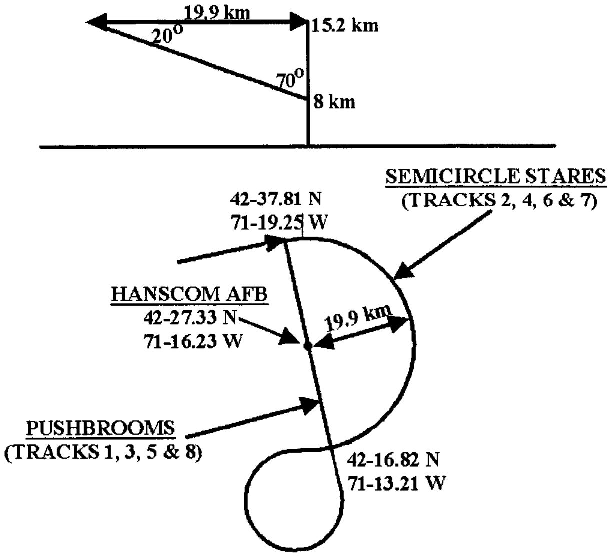

Figure 2. Collection trajectories over Hanscom AFB.

3. THEORY

In CloudDI, we use a linear least squares approach in order to calculate the fractional contribution of each template from a given basis set to a scene pixel spectrum of interest. In other words, if A is an m x n matrix of n templates (typically, spectra of various types of clouds and background features), S_{pix} is the m-element spectrum of the pixel of interest, and R is the resultant contribution vector, then clearly,

$$AR = S_{pix} \tag{1}$$

To solve for R, both sides of this equation are first multiplied by the transpose of A in order to create a system of normal equations [15]. The resultant vector can then be written,

$$R = (A^T A)^{-1} A^T S_{pix} \qquad (2)$$

Although evaluation of this expression without any constraints is straightforward if $A^T A$ is invertible, and is quite efficient using a high level programming language such as MATLAB [16], "unphysical" values are sometimes returned for the coefficient vector. Specifically, there is nothing in Eq. (2) that prevents negative values for R. One can constrain the solution by minimizing $AR - S_{pix}$ (the "error") for an R containing *positive* values only. MATLAB provides a built-in function for this purpose, "LSQNONNEG", which uses the non-negative least squares algorithm outlined in Lawson and Hanson's text [17]. In Section 4, we compare the speed and the results of the implementation of both the unconstrained LLSQ algorithm and the constrained (non-negative) version on ARES data. It should be noted that we make one further modification to these algorithms in order to reduce the impact of the data measured in the reflective versus thermal spectral regions by (linearly) weighting the data in the thermal bands higher than those in the reflective bands. We have added this weighting step to CloudDI, as the variability of the reflective band data can be quite high due to even small changes in viewing geometry, cloud optical properties, and cloud topography. The variability of reflected radiance from different cloud types and different viewing angles is illustrated in Figure 3. These spectra were calculated using the HYPEX [18] software suite, which combines MOSART radiative transfer calculations with BRDF (bidirectional reflectance distribution function) look-up tables compiled for a variety of clouds and background materials at different angles. HYPEX was also employed to calculate our templates for the LLSQ " A " matrix in refs. [5&6].

4. RESULTS

In our effort to calculate suitable cloud templates for use in CloudDI analyses, we studied the cloud modeling capabilities of three spectral radiance calculators, MODTRAN (V.4, Release 2), MOSART (V.1.60), and the MOSART-based HYPEX (V.1.5). In HYPEX, MOSART is used to generate values for the incident radiation at different altitudes, based upon input geometric and atmospheric parameters. The MOSART atmospheric background file (the binary ".bck" file), is then combined with data from the HYPEX spectral database for a given material (e.g., cloud, soil, vegetation...) in SPCALC, a HYPEX program that calculates radiative transport. MOSART itself may be used to model radiative transport through clouds. In this case, MOSART's own spectral databases and radiative transport models are employed.

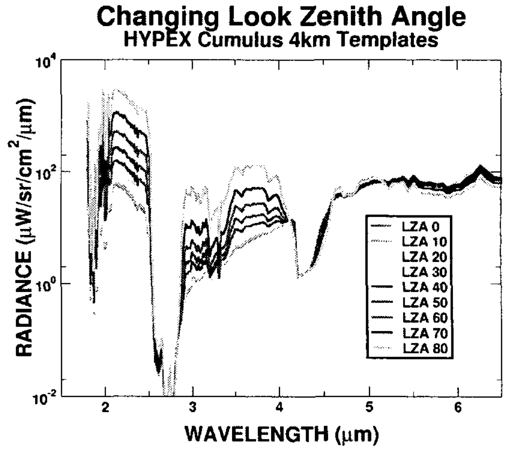

Figure 3. HYPEX - generated spectra for cumulus clouds at different viewing geometries. The observer-sensor azimuth is 170°, the solar zenith angle is 83.75°, and the solar azimuth is 268°. The azimuth angles are measured East of North.

One type of cloud template we were especially interested in generating for use in CloudDI was one containing multiple layers of clouds (e.g., a 1 km thick cirrus cloud over a 2 km thick cumulus cloud). We soon found that the only one of these programs to address multiple layer modeling *explicitly* is MOSART, which allows one to specify both a low-altitude cloud and a high-altitude cirrus cloud simultaneously in its 'hydrometeor' section[†]. The problem with using MOSART to calculate these characteristic cloud radiance values, however, is its speed. Using one R10000 processor of a Silicon Graphics Octane workstation, it can take up to 6 hours to execute one such MOSART calculation over a wide spectral range (e.g., from 0.4 μm in the visible, through 6 μm in the MWIR). Use of HYPEX mitigates the speed problem, as the cloud radiances are calculated via the SPCALC program based upon interpolations from values in BRDF databases (which are included in the HYPEX package). Moreover, using HYPEX, multiple cloud templates may be quickly (typically 10 seconds) calculated based upon only one MOSART background file. The calculation of the spectral signatures for 10 clouds and terrain features generally requires about 1.5 to 2 hours of computation time using HYPEX. A quick summary of the main differences between MODTRAN, MOSART, and HYPEX are delineated in Table 1.

[†] Layers of clouds may also be modeled using MODTRAN 4 if the user turns on the NCRALT input in card 2A and enters the cloud data at the desired altitudes manually (i.e., liquid water content, ice water content, and rain rate).

Table 1. Summary of main differences between spectral radiance calculators, MODTRAN, MOSART, and HYPEX

MODTRAN	MOSART	HYPEX
FAST (in LOWTRAN mode) LOWTRAN: 14 s.[‡] MODTRAN: ISAACS: 59 s. DISORT: 10 min.	**SLOW** 3 hrs., 6min.	**SLOW** BUT, only small penalty for multiple templates MOSART .bck: 58 min., 11 sec. SPCALC: ~10 sec.
DISORT or ISAACS Multiple scattering algorithm Multistream capability	APART or ISAACS Multiple scattering algorithm	APART Multiple scattering algorithm
- 12 Cloud models - Can adjust alt., thick., extinction - V.4 multiple clouds (manual data input)	- 20 Cloud models - Can adjust alt., thick., extinction - Multiple clouds	- 4 Cloud models - Can adjust alt. - No mult. clouds - BRDF database

Currently, the calculation of multiple-cloud-layer templates is not supported by HYPEX. To circumvent this problem, we modified the MOSART input file used by HYPEX to include a "hydrometeor" section, added a thin layer (1 km thick, extinction coefficient = 0.14 km^{-1}) of cirrus clouds, ran MOSART, and finally ran SPCALC on the MOSART output. In Figure 4, we compare a MOSART run in which we calculated the total radiance from layers of 2 km cumulus clouds and 6 km cirrus clouds with the MOSART-HYPEX result. In the VIS through SWIR, the MOSART-alone calculation falls below the HYPEX result. In the MWIR, on the other hand, the MOSART calculation is lower than the HYPEX run. One explanation for the differences may be that thickness of the HYPEX cumulus cloud was not equivalent to the thickness of the cumulus cloud in the MOSART calculation. The thickness of the cumulus cloud model is not clearly documented in the HYPEX software package.

Despite the differences between the MOSART-alone and the MOSART-HYPEX multiple-layer templates, they both illustrate the effects of an intervening cirrus cloud layer upon radiance calculations for low-altitude clouds. In Figure 5, for example, it is evident that the (MOSART-generated) cumulus clouds at both 1 and 3 km base altitudes are associated with larger radiance values in the reflective 2.2 μm band than the cumulus clouds at the same altitudes but under a layer of thin cirrus clouds (1 km thick, extinction coefficient = 0.14 km^{-1}). In the 4.8 μm spectral region, on the other hand, the altitude of the cloud appears to be of greater importance in determining radiance values than the cirrus cloud transmission factor. In this region, the radiance of both 1 km clouds (with and without a thin cirrus layer overhead) is higher than the radiance of both 3 km clouds. The cirrus cloud at 6 km is shown simply as a benchmark.

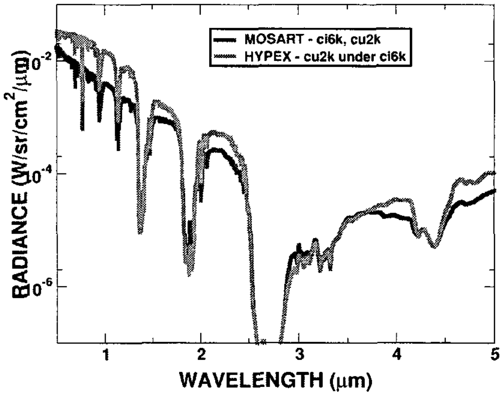

Figure 4. Comparison of multiple layer template calculations using either MOSART alone or MOSART with HYPEX under space-based viewing conditions.

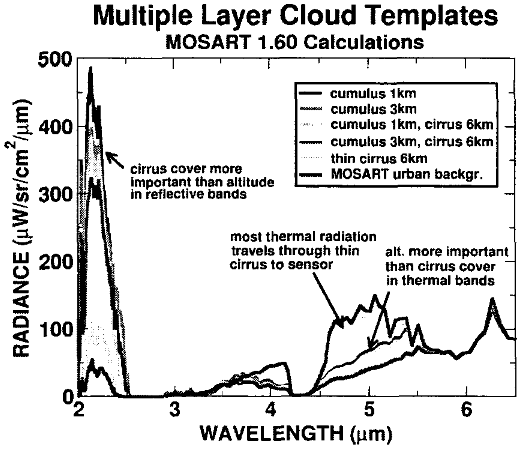

Figure 5. Comparison of multiple-layer versus single-layer spectral signatures for selected clouds. Calculations were carried out using the MOSART midlatitude summer atmosphere under the Hanscom nadir viewing conditions. The MOSART urban background was used in all calculations.

As a test of method, we calculated several single-layer cloud templates and a 2-layer template using MODTRAN[§] and ran

[‡] Models were run over the frequency range 1515 cm^{-1} to 5555 cm^{-1} and one cloud template was calculated in each case using a Silicon Graphics Indigo 2 workstation with a R4400, 250 MHz processor and 2 MB 2° cache. Isaacs multiple scattering was included in the LOWTRAN run.

[§] The multiple layer, "hybrid" template was calculated by turning on the NCRALT input in Card 2A, inputting the LWC and IWC information from the Tape 6 output of a previous single layer cumulus 4km run, and adding an ice

CloudDI on a scene containing multiple cloud layers. We were especially interested in whether CloudDI required the multiple-cloud-layer template in order to detect layers of clouds or whether several single-layer cloud templates would do the job. The spectra we employed for this experiment contained 1 km thick cumulus clouds at both 4 km and 7 km base altitudes, was viewed at a 45° LZA, and was a day scene (solar zenith angle (SZA) = 58°) in the winter. In Figure 6, we plot the spectrum (at the bands used in the analysis) of "in-scene" cloud pixels along with the cloud templates we calculated. It is evident that none of the calculated templates match the points from the in-scene cloud pixels exactly, indicating a need for adjusting the parameters in the templates. The fit between templates and data, *is* good enough to provide for encouraging CloudDI analyses, however.

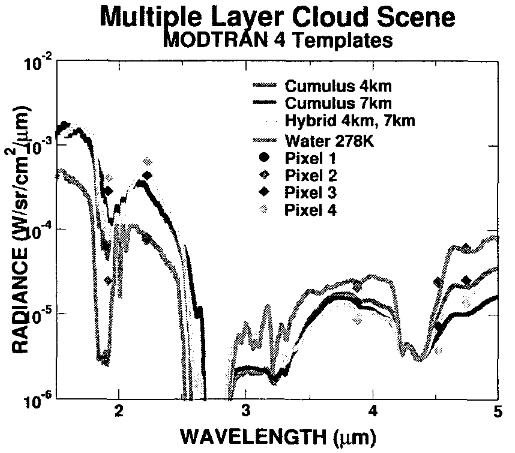

Figure 6. MODTRAN templates used in CloudDI analysis of scene containing multiple cloud layers.

CloudDI was run on the scene described above with the templates shown in Figure 6 excluding the water template, which is shown merely as a point of comparison (an in-scene terrain pixel was used instead). In Table 2, the CloudDI results are compared with ground truth at selected pixels. The ground truth data consist of radiosonde and radar measurements. Confidence levels are reported as "conf. A" = confident, "conf. B" = fairly sure, and "conf. C" = sketchy. CloudDI was run on these data under two different sets of conditions: In Run 1, 4 templates (cumulus at 7km, cumulus at 4km, a "hybrid" cumulus at 4km under a thin ice cloud at 7km (0.00143 g/m^3 ice), and an in-scene water pixel) and 5 bands (1.85, 2.2, 3.9, 4.55, and 4.75 μm) were employed. In Run 2, the same bands were used, but the "hybrid" template was removed. Perhaps the most obvious result of these analyses is that CloudDI typed both Pixels 1 and 2 virtually the same way – as mostly terrain, but with some cloud aspect. In Run 1, the cloud is chosen to have multiple layers, in agreement with the ground truth data. When the multi-layer cloud template is removed in Run 2, however, the cloud in Pixels 1 and 2 is typed as a cumulus cloud at 4 km. As for why Pixels 1 and 2 are given almost identical template coefficients by CloudDI, the explanation is apparent upon examination of the pixel data points: These pixels essentially overlap at the bands used in the analysis. It is possible that there were, in fact, traces of clouds in the "clear" pixel that CloudDI picked up but that the ground truth did not. In both Runs 1 and 2, CloudDI correctly typed Pixels 3 and 4 as a cloud with an altitude of 7km.

Table 2. Summary of CloudDI Results for Multiple Layer Cloud Scene. In Run 1, 4 templates were employed: cum 7km, cum 4km, cir 7km & cum 4km, and an in-scene terrain spectrum. For Run2, the "hybrid" template was removed.

	Ground	Run 1	Run 2
Pixel 1	Clear Conf. B	0.09 hy 4,7km 0.91 ter	0.13 cu 4km 0.87 ter
Pixel 2	4km, 7km Conf. A	0.10 hy 4,7km 0.90 ter	0.13 cu 4km 0.87 ter
Pixel 3	7km Conf. B	0.94 cu 7km 0.06 ter	0.94 cu 7km 0.06 ter
Pixel 4	7km Conf. B	1.00 cu 7km	1.00 cu 7km

Cloud top temperature algorithm

There are currently several different methods for extracting cloud altitude information from spectral scene data, some of which are summarized above in Section 1. Here, we propose the use of a technique for remotely calculating temperature similar to that described in Reference [4] in order to complement CloudDI calculations. Implementation of this algorithm within the CloudDI framework might, for instance, help restrict the possible templates to a few "best guesses" (thereby eliminating some computation time).

Specifically, this cloud-top temperature algorithm would work in the following way: First, the path radiance and transmittance is calculated via MODTRAN or MOSART in the 4.6 to 4.9 μm ARES bands, based upon the user-supplied conditions of the data collect (e.g., latitude, longitude, season, visibility, etc.). This calculation is the same as that done for the CloudDI template preparation. The path radiance is then subtracted from the ARES band data for a selected pixel. After dividing the resulting value by the path transmittance and the emissivity of the cloud (approximated using empirical data), the effective temperature may be gleaned by comparing the resulting radiance values with Planck distributions.

At night, the effective temperature calculated in this way should be close to the actual temperature of the cloud, depending upon how accurately the path radiance and

cloud with an IWC of 0.00143 g/m^3 between 7 and 8 km altitude.

atmospheric transmission are known. Since the thermal radiation is around an order of magnitude greater than the solar reflected radiance in the 4.6 to 4.9 μm band under non-specular viewing conditions, the effective temperature calculated during the day for a single layer cloud should be similar to the actual temperature, varying more or less depending upon the viewing geometry. Once a cloud top temperature is calculated, the cloud's approximate altitude can be deduced based upon statistical sounding data. The altitude data can then be used to create a select group of HYPEX templates for a subsequent CloudDI analysis of the entire scene.

Cloud/no cloud masks

One important consideration in performing these cloud characterization analyses is the time necessary for completing the necessary calculations. Often, providing great detail about the clouds in a particular scene is not required and simpler, less time-consuming algorithms may be substituted for the more accurate, but more time-intensive ones. In this case, the calculation of a simple cloud/no cloud mask might be appropriate.

CloudDI cloud/no cloud masks

In our studies of the CloudDI algorithm, we have experimented with using both a constrained version (in which the resultant vector is calculated to minimize the error in $AR - S_{pix}$, but is constrained by the requirement that all its values be positive) and an unconstrained version. Use of the unconstrained version often results in "unphysical" values for R when the system is effectively overdetermined (i.e., when a large number of similar templates are included in the calculation). In our previous CloudDI papers, we concentrated exclusively on the constrained implementation. This made sense at the time, as we were looking at single representative pixels, and the time required for the multiple iterations of least squares fitting associated with the constrained algorithm is not excessive for a one-pixel analysis. Use of the constrained algorithm on an entire scene (containing 45 x 750 = 33,750 pixels, for the Hanscom ARES collects – one field of view, or 65,536 pixels for a 256 x 256 SSGM scene), however, takes tens of minutes as opposed to tens of seconds for the unconstrained version. Thus, we were anxious to discover whether the unconstrained algorithm might be useful in some situations.

We found, in fact, that if a minimal set of templates is employed, the unconstrained CloudDI algorithm works just as well as the slower constrained version. So, if only 3 templates are used (a high altitude cloud, a low altitude cloud, and water, for example) in order to create a simple cloud/no cloud mask, the unconstrained CloudDI can return results similar to the constrained CloudDI, in about 1/50th of the time. In Figure 7, we compare a cloud/no cloud mask created by the unconstrained CloudDI and one created by the constrained algorithm with an image from the 3.9 μm ARES band (channel 45), in which the cloud cover is quite visible at the top of the image. At the bottom of the image, various terrain features such as streets can be seen. It is apparent that the unconstrained CloudDI mask contains a greater number of cloudy pixels than the constrained mask, which in turn appears to more closely correspond to the channel 45 ARES image. For some applications, however, the overdetermination of cloudy pixels is desirable, in which case the unconstrained CloudDI mask would be preferable. Both the constrained and unconstrained CloudDI experiments shown here exploited data from 5 ARES bands. The constrained calculation took almost 30 minutes whereas the uncontrained algorithm ran 41 seconds.

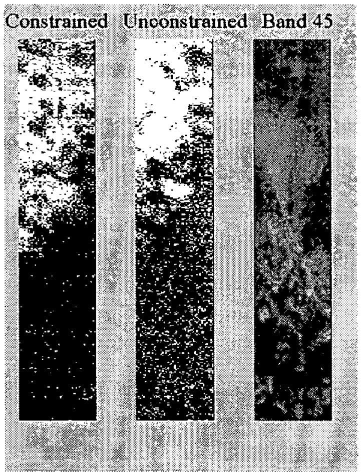

Figure 7. Cloud/no cloud mask as calculated via constrained and unconstrained CloudDI implementations.

Combination SAALT and CloudDI analysis

Another option for quickly analyzing a scene is to first cluster it into groups of pixels with similar spectral signatures using a method such as SAALT, and then further analyzing (identifying) the clusters using CloudDI. When a scene is clustered by SAALT, a "cluster center" (band-by-band average spectrum) is calculated for each group of pixels. Thus, by first clustering the scene using SAALT, only a few average spectra need to be processed by CloudDI, thereby cutting into the calculation time significantly.

Therefore, if information beyond a simple cloud/no cloud mask is desired, it is useful to run SAALT with a large maximum number of clusters (typically increasing the run time from ~0.5 min. to ~2 min.), which may then be identified using the constrained CloudDI with an appropriate selection of templates. The number of CloudDI templates is bounded only by the number of spectral bands used in the analysis. With the effective number of pixels reduced from tens of thousands to less than ten, even the constrained CloudDI runs quickly (less than 1 minute).

Algorithm efficiency and accuracy

The two major sources of computation time associated with CloudDI are the template calculation and the iterative computations associated with the constrained algorithm when entire scenes containing tens of thousands of pixels are processed (as discussed above). By preprocessing the scene with a clustering procedure such as SAALT, the cpu time required for running CloudDI may be reduced significantly. This leaves the template calculation as the major time sink in the CloudDI method.

In an effort to reduce the time associated with this step of the process, we have investigated the possibility of using MODTRAN instead of MOSART (or the MOSART-based HYPEX) for our calculations. For the same type of calculation, we have found that MODTRAN (in low-resolution "LOWTRAN" mode) runs approximately fifty times faster than MOSART. Thus, a 2 hour MOSART run is reduced to less than 2 minutes in MODTRAN. Despite the desirable decrease in computation time associated with MODTRAN, however, there are currently several benefits to continuing on with MOSART. One of these is MOSART's hydrometeor section, which allows one to specify a cirrus cloud in addition to a low altitude cloud of several different types. This capability is useful in the preparation of multiple layer cloud templates.

In the "Addendum to Moderate Spectral Atmospheric Radiance and Transmittance (MOSART) Computer Code," [19] Cornette, et al., include a section on their study comparing MOSART with MODTRAN. In this study, the authors ran MOSART 1.5 under the conditions specified in the 15 test cases included with the MODTRAN 3.7 distribution and compared the MODTRAN and MOSART results. They found that in the most extreme cases the transmittances calculated by the two programs differed by up to 30% and the radiance values differed by up to 25%. Typically, the results of the two programs were more in accord (differing from ~1% to 10%). Cornette, et al. explain that these differences arise due to several factors, including differences in the structure and databases of the codes and in some of the algorithms themselves. For instance, MOSART, they write, has a higher resolution altitude grid than MODTRAN, which results in different extinction coefficients. This accounts for some of the differences between MODTRAN and MOSART's transmission calculations. Another difference between MODTRAN and MOSART is their multiple scattering algorithms. MODTRAN uses either the Isaacs two-stream algorithm or the DISORT algorithm (discrete-ordinate-method radiative transfer) [20]. MOSART, on the other hand, employs the APART multiple scattering method if the "multiple scattering" option is turned on and the Isaacs 2-stream method if it turned off [21].

In Ref. [22], MODTRAN 3.7 and MODTRAN 4 cloud model and multiple scattering upgrades are outlined. In both of these versions, the user may model clouds at chosen altitudes and thicknesses. Furthermore, according to [22], multiple layers of overlapping and non-overlapping clouds may be specified in both MODTRAN 3.7 and MODTRAN 4. This multiple cloud 'option', however, is not documented in the MODTRAN User's Manual, and we have not been able to use it. The main upgrade in MODTRAN 4 is the addition of a correlated-k capability. Essentially, this feature converts the MODTRAN band model calculations into a set of equivalent monochromatic calculations, thereby preserving the accuracy of a linear-in-tau approximation [22]. This upgrade should therefore improve the accuracy of the multiple scattering calculations in MODTRAN version 4.

We ran a few test cases of our own in order to try to quantify the differences in cloud modeling between MODTRAN, MOSART (and HYPEX) under the type of conditions typical to the Hanscom ARES collects. In Figure 8, we show one such test case in which 1 km thick cirrus clouds, with a base altitude of 8 km and an extinction coefficient of 4.1 km^{-1} are compared under nadir viewing conditions. A midlatitude summer atmosphere was used in all the runs. It is evident in this plot that the MOSART and MODTRAN results agree quite well in the SWIR and MWIR and differ by almost 50% in the 2.2 μm reflective band. This difference decreases when the model 19 ("subvisual") cirrus cloud is used in MODTRAN instead of the model 18 ("standard cirrus") cloud. However in this case, the comparison in the thermal bands degrades. MODTRAN calculations were done using both the Isaacs (2-stream) and the DISORT (multi-stream) multiple scattering algorithms, although in this case there is apparently little difference between the two calculations. The HYPEX results differ significantly from the other two in the SWIR and 2.2 μm band.

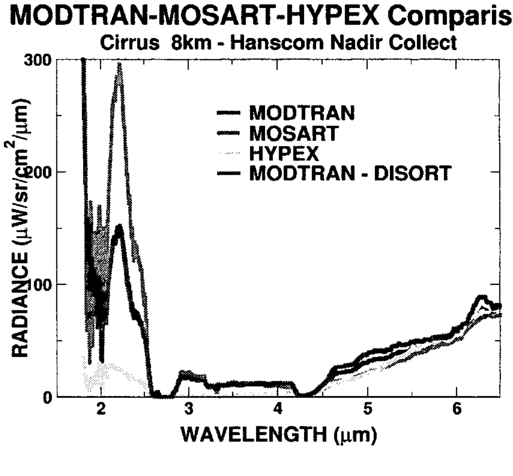

Figure 8. Comparison of MODTRAN, MOSART (and HYPEX) under nadir viewing conditions for a cirrus cloud at 8 km.

In Figure 9, we compare the results of calculations using the three programs to calculate the spectral signature of a cumulus cloud with a base altitude at 4 km. Here, once again, the MODTRAN and MOSART plots are fairly close when the MODTRAN cloud signature is calculated with the Isaacs 2-stream multiple scattering algorithm. When the DISORT multiple scattering algorithm is used in the MODTRAN calculation, however, the MODTRAN- and HYPEX-generated spectra compare favorably. Despite good matches between the MODTRAN and MOSART cumulus cloud spectra in the region below 4 μm and above 6 μm, there is a 34% difference between the two spectra at 5 μm. This difference disappears if the MOSART cumulus cloud spectrum (with a specified altitude of 4 km and thickness of 2 km) is compared with the spectrum of a MODTRAN altostratus cloud calculated with the Isaacs multiple scattering algorithm. The MOSART and MODTRAN altostratus and cumulus clouds corresponding to the parameters described above are plotted together in Figure 9. Interestingly, the best match is between the MODTRAN altostratus and the MOSART cumulus clouds.

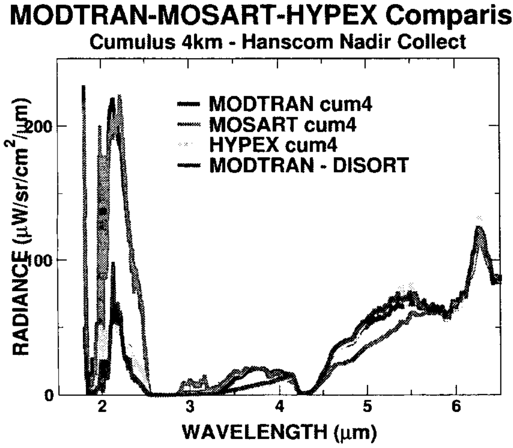

Figure 9. Comparison of MODTRAN, MOSART, and HYPEX models for a 2 km thick cumulus cloud with a base altitude of 4km.

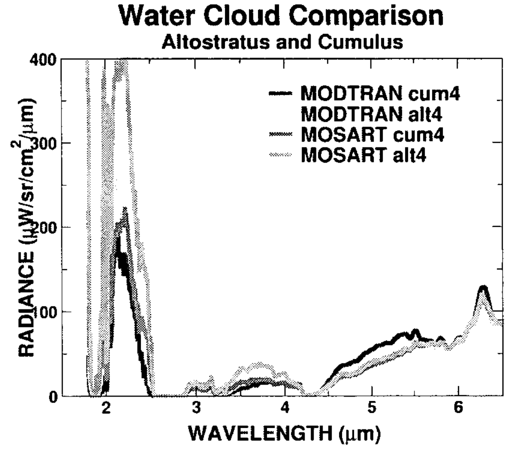

Figure 10. Comparison of MODTRAN and MOSART cumulus and altostratus clouds. The observation parameters for these calculations are the same as those employed for the Hanscom nadir collects. MODTRAN was run using the Isaacs two-stream multiple scattering method.

In ref. [5], we showed results from running CloudDI on pixel spectra from both nadir-viewed Hanscom AFB scenes and from scenes viewed at an LZA of 70°. It was found that although CloudDI returned results that coincided fairly well with ground truth data for the 70° LZA data, it failed to detect (cirrus) clouds in some of the nadir-viewed scenes. It is probable that this failure was due in part to the templates calculated with the HYPEX software, which only provides an optically thick cirrus model. This means that in HYPEX, all high-altitude clouds are associated with relatively low radiance values (which change with altitude) in the MWIR, as the thermal radiance from the ground does not reach the sensor through the clouds. In order to illustrate this point, we plot the (MODTRAN-calculated) spectral signatures of "thick" cirrus clouds (1 km thick with an extinction coefficient of 4.1 km^{-1}) and "thin" cirrus clouds (also 1 km thick, but with an extinction coefficient of 0.14 km^{-1}) at varying altitudes as well as a terrain background spectrum in Figure 11. It is clear upon inspection of this figure that under the given set of conditions there is virtually no difference between the spectral signatures of optically thin cirrus clouds at different altitudes. Furthermore, in the MWIR, the radiance values are greater for the thin cirrus clouds than for the optically thick clouds despite similarities in altitudes.

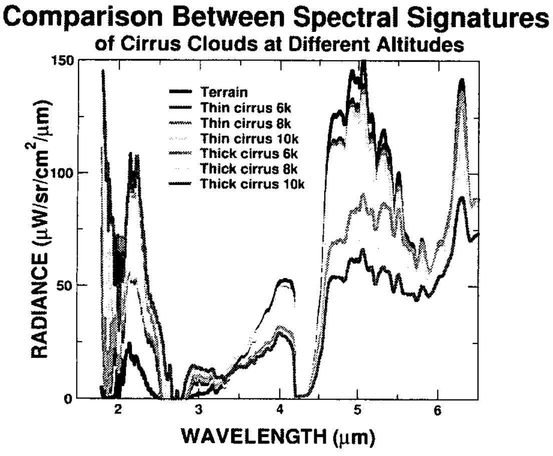

Figure 11. Comparison of the MODTRAN-calculated spectral signatures of optically thick and optically thin cirrus clouds.

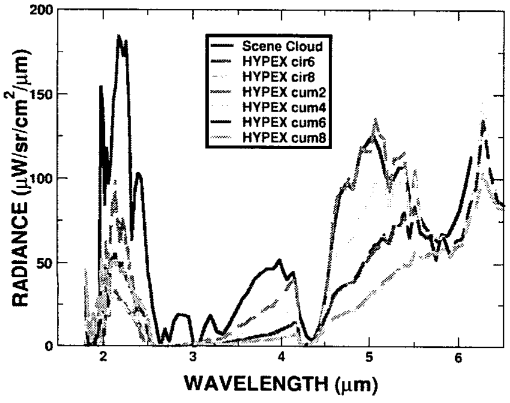

Figure 12. HYPEX templates calculated for the nadir-viewed Hanscom scene.

In Figure 12, HYPEX templates calculated for the Hanscom nadir-scanned ARES data are plotted with a "cloud" pixel taken from the scene. It is evident that none of these templates match the scene data in every spectral region. In fact, the template that appears to match the in-scene cloud pixel the best is the cumulus 2 km template. This result disagrees with the ground truth radar data available for this collect (see Figure 13 below.).

According to the ground truth radar data for Hanscom on 16 September, 1995, the clouds above the AFB were thin cirrus clouds located approximately 6 km to 8 km above ground level. In an attempt to improve the templates for these ARES collects, new cloud templates were calculated using MODTRAN (LOWTRAN mode, Isaacs multiple scattering). In MODTRAN, one may specify cloud model, base altitude, thickness, and extinction coefficient. In Figure 14, MODTRAN templates calculated for a 1 km thick cirrus cloud at base altitude 6 km, with the default extinction coefficient (= thickness x 0.14 km^{-1}) and a 2 km thick cumulus cloud, with a base altitude of 4 km and the default extinction coefficient, are plotted along with a "cloudy" scene pixel and a "clear" scene pixel. It is apparent that the optically thin 6 km cirrus cloud calculated via MODTRAN matches the scene cloud spectrum quite well.

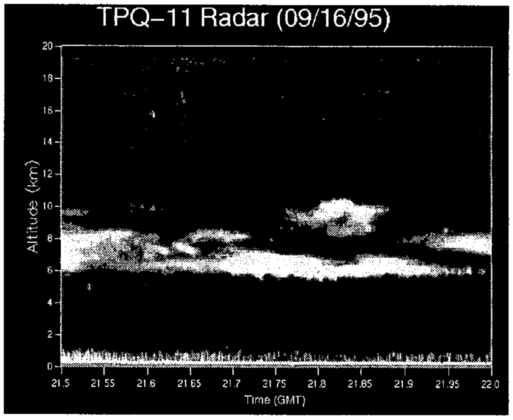

Figure 13. Radar data from Hanscom AFB on 16 September, 1995.

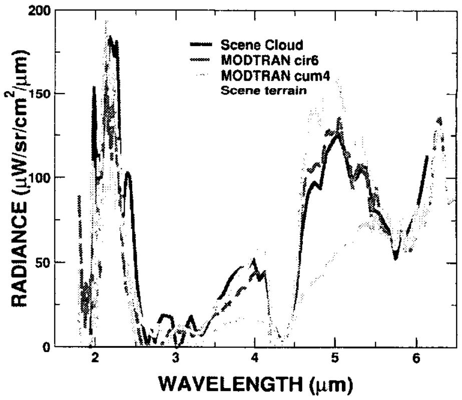

Figure 14. MODTRAN templates are represented by the 2 dashed lines and the scene cloudy and clear pixels are represented by solid lines.

We ran CloudDI using the new templates in both the constrained and unconstrained modes of operation and found that CloudDI now detects the thin cirrus clouds. In Figure 15, we present the results of one such CloudDI run. In this calculation, we used three templates: the MODTRAN cirrus 6 km cloud, the MODTRAN cumulus 4 km cloud, and the spectrum of a scene pixel predetermined to be clear. We ran the unconstrained CloudDI, and restricted the analysis to the 49 of the 75 available ARES bands with the best SNR values.

In this figure, the leftmost panel represents the percentage of the scene typed as cirrus cloud at 6 km. The bright pixels correspond to a high degree of correlation (a positive assignment). Thus, CloudDI has assigned most of the pixels in the upper portion of the image as cirrus clouds at 6 km. The second panel from the left is the corresponding image for the cumulus 4 km template and the middle panel is the terrain template image. When added together, the sum of the coefficients of each pixel represented in the three left-most panels equals 1 (after normalization). In general, the least squares fit is not perfect and the sum of the unnormalized coefficients does not equal 1. The second panel from the right is the image collected in the ARES band 45 (3.9 μm). The clouds are clearly evident in the upper half of this image. Finally, the residual image is displayed in the right-most panel indicating that the fit for the "bright" terrain features is the worst and that for the "dark" terrain features is the best (as it should be – the terrain template spectrum used in the calculation was a "dark" terrain pixel). The residuals calculated for the cloud pixels are typically 20-30%. The residual was calculated by taking the norm of the product of the template matrix and the coefficient vector minus the pixel spectrum (residual = $norm(AR - S_{pix})$). The results for running the constrained CloudDI algorithm under the same conditions look very similar to those displayed in Figure 15. The run-times for the two cases were not similar at all, however. Whereas the unconstrained CloudDI run took 116 seconds (~2 minutes), the constrained calculation stretched out 2,103 seconds (~35 minutes)**.

CloudDI was also run in both modes using the full resolution afforded by the ARES collects at Hanscom (i.e., using all 75 bands). It turns out that in this case, the algorithm performance actually degraded, as the low SNR in the 2.8 μm absorption band and the shorter wavelength region below 2.2 μm tended to skew the measured radiance values. Moreover, the 4.25 to 4.40 μm and 6.0 μm and longer channel radiance values were not robust either for various reasons.

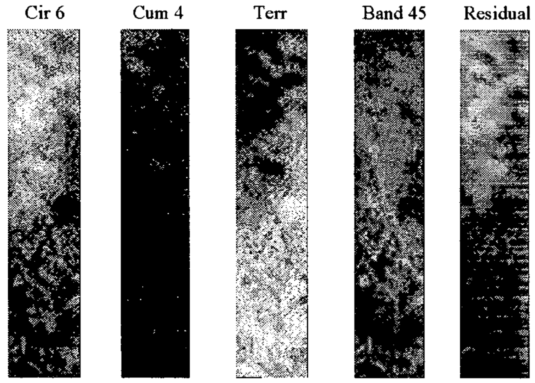

Figure 15. CloudDI results for the Hanscom track 1 (nadir) scene. From left to right: cirrus 6km, cumulus 4km, terrain, band 45 image, residual image.

We also ran constrained and unconstrained CloudDI (using the two MODTRAN cloud templates and one "terrain" template as described above) on our selected Hanscom scene using only 7 ARES bands. In this case, we employed the channel 13 (2.20 μm), channel 28 (2.79 μm), channel 45 (3.90 μm), channel 52 (4.45 μm), channel 53 (4.52 μm), channel 55 (4.67 μm), and channel 56 (4.75 μm) ARES bands. Under these conditions, both the constrained and unconstrained algorithms misassigned the clouds as cumulus 4 km, but nevertheless, did correctly discriminate between cloudy and clear pixels.

The cloud/no cloud masks presented above in Figure 7, were calculated using only 5 ARES channels: 1 (1.9 μm), 13, 45, 55, and 56. The channel 1 band was selected as it is located in an atmospheric absorption region, and therefore targets clouds at relatively high altitudes. The performance of the algorithms under these conditions was similar to the 7-band performance. Once again, the clouds were correctly discriminated from the clear pixels, but were misidentified as low-mid altitude cumulus clouds.

In the CloudDI experiments described above, only three templates were employed. As there are significant differences between these spectra and they do not comprise an overdetermined basis set, the constrained and unconstrained CloudDI results are very similar. The results returned by the two algorithms diverge as soon as additional templates are added. The use of multiple templates is desirable in cases where the characteristics of the cloud layer or layers is completely unknown. When multiple templates are used, however, the unconstrained CloudDI algorithm tends to fail (i.e., return "unphysical" results – negative values). Therefore, when multiple templates are required, use of the constrained algorithm, which returns only "physical" results, becomes worth the additional cpu time. In Figure 16, we present constrained and unconstrained CloudDI runs in which 7 cloud templates and

** We should note that these calculations were done using MATLAB, which (unlike C or FORTRAN) does not compile the entire program before running. Therefore, many unnecessary steps are repeated in routines containing FOR loops such as the constrained CloudDI algorithm. It is very likely that an implementation of the constrained CloudDI algorithm in C would be quite a bit more efficient than the current MATLAB implementation.

1 terrain template were employed. These templates consist of a: thin cirrus cloud at 6 km over land, thick cirrus clouds at 6 and 10 km, cumulus clouds at 2, 4, 6 and 8 km, and an in-scene terrain pixel spectrum. All of the cloud spectra were calculated with MODTRAN in LOWTRAN mode (reduced resolution). We ran both versions of CloudDI using 49 bands and using 8 bands (ARES channels 1, 13, 28, 45, 52, 53, 55, and 56). Recall that the minimum number of bands that is required for executing the CloudDI algorithm with 8 templates is 8 as explicated in Section 3 above.

In this figure we show the results for the templates corresponding to the CloudDI assignments only. In both the full (panel A) and degraded (panel C) resolution runs, the clouds were correctly distinguished from the terrain features and were assigned as cumulus clouds at 8 km by the constrained algorithm. Under the reduced spectral resolution condition, CloudDI also assigned some of the cloud and terrain pixels as "thick cirrus 10k clouds". The cumulus 8k plus the cirrus 10k results are added together and shown as "all clouds" in the middle image in panel C. It is interesting that CloudDI did not assign the clouds in these calculations to the thin cirrus template. Apparently, the optimal assignment for the cloud pixels under these conditions was as 50-60% cumulus cloud at 8km and the rest terrain or high altitude cirrus (in the reduced resolution run). In general, the cloud pixels were not correctly distinguished from the terrain pixels by the unconstrained algorithm in either the full (panel B) or degraded (panel D) resolution cases.

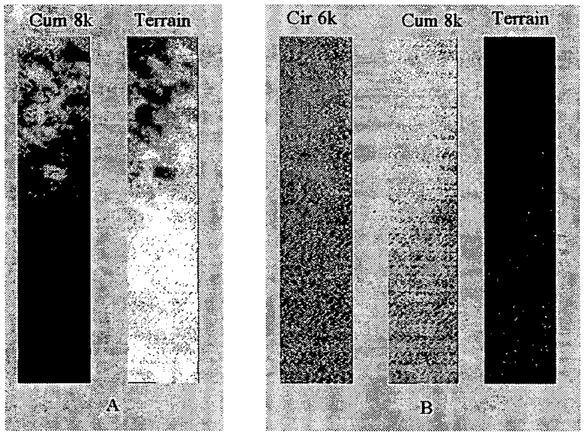

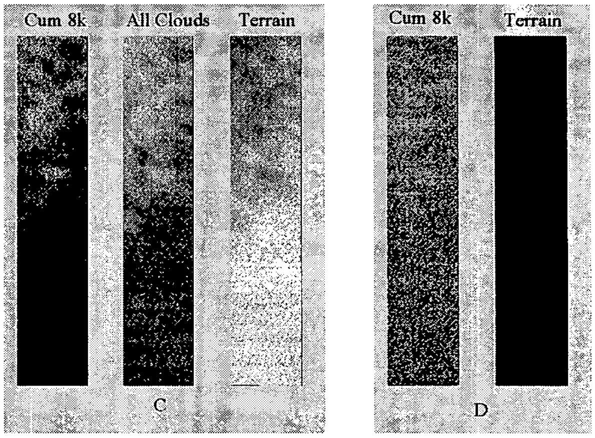

Figure 16. CloudDI Results for multiple template runs. Panels A & B are full resolution and C & D are reduced resolution.

In Table 3 and Table 4, we summarize the run times and the results of our CloudDI experiments on the Hanscom ARES data.

Table 3. CloudDI Results Using 3 Templates

Algorithm	No. Bands	Time	Results
Constr.	75		
Unconstr.	75	145 sec.	good

Algorithm	No.Bands	Time	Results
Constr.	49	2103 sec.	excellent
Unconstr.	49	116 sec.	excellent

Algorithm	No.Bands	Time	Results
Constr.	7	1989 sec.	fair
Unconstr.	7	43 sec.	fair

Algorithm	No.Bands	Time	Results
Constr.	5	1789 sec.	fair
Unconstr.	5	41 sec.	fair

Table 4. CloudDI Results Using 8 Templates

Algorithm	No.Bands	Time	Results
Constr.	49	2021 sec.	good
Unconstr.	49	120 sec	poor

Algorithm	No.Bands	Time	Results
Constr.	8	2041 sec.	good
Unconstr.	8	50 sec	poor

5. CONCLUSIONS and FUTURE DIRECTIONS

In the preceding pages, we have described our latest work using the CloudDI least squares method to discriminate cloudy from terrain pixels and to characterize the clouds in scenes comprised of remote sensing spectral data in the S/MWIR. In general, CloudDI consists of two main parts: The construction of templates and the comparison of these templates to the spectra of scene pixels. In the process of learning to construct complicated cloud templates, we were compelled to compare various spectral radiance calculators, including MODTRAN, MOSART, and HYPEX in terms of quality of results, calculation efficiency, and the extent and flexibility of the modeling resources available in each.

What we found is that in most cases, MODTRAN is quicker than either of the other two programs and is of sufficient accuracy (even using the less-accurate Isaacs two-stream multiple scattering calculation method) for constructing CloudDI templates at the bands of interest. In some situations, desirable features available in MOSART such as the capability for easily modeling multiple clouds and the flexibility in constructing model atmospheres are possibly worth the additional computation time. Although HYPEX has a lot to offer, perhaps, in terms of its BRDF databases, there are several bugs in the program that result in the calculation of negative radiance values under some conditions. Furthermore, the omission from HYPEX of a capability for modifying cloud thickness and extinction coefficients is a serious impediment to its use in the calculation of cloud templates for CloudDI.

In Section 4, we presented the results of experiments in which we constructed a multi-cloud template using MODTRAN and used it in a CloudDI analysis. Although it is not clear at this time whether or not these multiple-layer templates are necessary for our studies, it is apparent that attempts to model multiple-cloud scenes push the limits of the existing tools and are, in any case, helpful in elucidating the interaction between clouds and S/MWIR radiation.

We also proposed a method for calculating cloud top temperatures using data from the 3.9 to 4.3 μm spectral region. This method would complement CloudDI either by narrowing the set of templates, or by confirming or resolving existing CloudDI analyses. We have begun work on implementing and testing this procedure in CloudDI and will report our results as they become available.

For the first time, we have shown the results of analyzing entire scenes, each containing thousands of pixels using CloudDI. In an effort to increase the speed of these calculations, we experimented with using an unconstrained least squares algorithm, which does not require the iterative calculations necessary in the constrained version. We found that although the unconstrained CloudDI is quite a bit faster than the constrained version, it often yields "unphysical" results, especially if multiple templates are used. The unconstrained CloudDI is most useful when the information content required of the analysis is relatively low (i.e., a simple cloud/no cloud mask or even the discrimination between low altitude water clouds, high altitude ice clouds, and terrain).

With some of the template construction issues resolved and the algorithm itself more or less optimized, CloudDI now needs to be tested under a broad range of conditions. For example, we have just begun to analyze night scenes using CloudDI. Since at night, all reflective bands are basically useless, only thermal bands can be employed in the CloudDI calculations. Thus, a new set of bands must be chosen for these analyses. Furthermore, we have not yet tested CloudDI on scenes containing significant amounts of ice or sand, both of which have spectral properties that are similar to those of clouds under some conditions.

REFERENCES

[1] K. Brower, "Optical Transmission of Light Through Clouds," Sandia Report #SAND97-1139 • UC-703, May 1997.

[2] K.L. Brower, "Apparent Spatial Blurring and Displacement of a Point Optical Source Due to Cloud Scattering," Sandia Report #SAND97-2164 * UC-703, Spetember, 1997.

[3] G.B. Gustafson, et al., "Support of Environmental Requirements for Cloud Analysis and Archive (SERCAA): Algorithm Descriptions," Report #PL-TR-94-2114, Phillips Laboratory, Directorate of Geophysics, Air Force Material Command, Hanscom Air Force Base, MA, 28 March, 1994.

[4] B. Ben-Dor, L.S. Balfour, and A. Pasternak, "Utility of the 4.6- to 4.9-μm atmospheric window for remote sensing of background temperature," Opt. Engin., **33**(9), 3056 (1994).

[5] M.A. Najarian, T.J. Slusarchyk, J.J. Lisowski, and D.E. Sene, "Cloud Detection and Altitude Estimation in the S/MWIR Utilizing ARES Data," *1998 IEEE Aerospace Applications Conference Proceedings*, March 1998.

[6] M.A. Najarian, B.J. Borowski, M.Hryszko, J.J. Lisowski, and D.E. Sene, "Impact of Reduced Spectral Resolution on Cloud Detection and Altitude Estimation," *1999 IEEE Aerospace Applications Conference Proceedings*, March 1999.

[7] A. Weisberg, M. Najarian, B. Borowski, J. Lisowski, and B. Miller, "Spectral Angle Automatic cLuster rouTine (SAALT): An Unsupervised Multispectral Clustering Algorithm," *1999 IEEE Aerospace Applications Conference Proceedings*, March 1999.

[8] H.K. Burke, S.M. Hsu, M.K. Griffin, and A.T. Stair, "Application of Hyperspectral Sensing to Surveillance and Atmospheric Sounding," Report under Air Force contract F19628-95-C-0002.

[9] S.C. Ou, K.N. Liou, P. Yang, P. Rolland, T.R. Caudill, J. Lisowski, and B. Morrison, "Airborne retireval of cirrus cloud optical and microphysical properties using Airborne Remote Earth Sensing System 5.1-5.3 and 3.7-µm channel data," J. Geophys. Research, **103**(D18), 23231 (1998).

[10]I.S. Robinson, RADEX, inc., "SBIRS Phenomenology Exploitation Program, Data Collection and Analysis Plans," May, 1996.

[11]I.S. Robinson, RADEX, Inc., "SBIRS Phenomenology Exploitation Program, ARES Data Collection Plan," May, 1996.

[12] "ARES Mission Summaries for 1995 SBIRS PEP Experiments," SciTec, Inc., March 1996.

[13] "ARES Mission Summaries for 1996 SBIRS PEP Experiments," SciTec, Inc., March 1997.

[14] A.B. Ritter, M.A. Najarian, J.R. Howell, E.R. Dunn, and J.J. Lisowski, "Data Analysis Report, Hanscom AFB, September 16, 1995," SciTec, Inc., March 1997.

[15] G. Strang, Linear Algebra and its Applications, 3rd Ed., Harcourt Brace Jovanovich, Inc. San Diego, 1988.

[16] MATLAB, version 5.3.0, The Mathworks, Inc. January 21 1999.

[17] Lawson and Hanson, Solving Least Squares Problems, Prentice-Hall, 1974.

[18] Hyperspectral Exploitation Toolkit (HYPEX) Version 1.5, PRA, Inc., San Diego, CA, 1999.

[19] W.M. Cornette, A. Berk, and S.J. Westmoreland, "Addendum to Moderate Spectral Atmospheric Radiance and Transmittance (MOSART) Computer Code," 31 December, 1997 (included with MOSART v. 1.6 distribution).

[20] K. Stamnes, S-C. Tsay, W. Wiscombe, and K. Jayaweera, "Numerically stable algorithm for discrete-ordinate-method radiative transfer in multiple scattering and emitting layered media," Appl. Opt. **27**, 2502 (1988).

[21] W.M. Cornette, "Moderate Spectral Atmospheric Radiance and Transmittance Program (MOSART) Version 1.30 Vol. III: Technical Reference Manual, December 1994

[22] A. Berk, L.S. Bernstein, G.P. Anderson, P.K. Acharya, D.C. Robertson, J.H. Chetwnnd, and S.M. Adler-Golden, "MODTRAN Cloud and Multiple Scattering Upgrades with Application to AVIRIS," Remote Sens. Environ., **65**, 367 (1998).

BIOGRAPHY

Jennifer Davis *recently started work as a scientist at SciTec, Inc. after completing a Ph.D. in femtosecond chemistry at Princeton University. The focus of Jennifer's thesis work was ultrafast (picosecond and femtosecond) lasers and their applications in chemsitry and high-speed communication systems. Since arriving at SciTec, she has shifted her attention to cloud physics ("and she's had her head in the clouds ever since..."). Currently, she is working on developing algorithms for analyzing remote sensing data in a variety of spectral bands. Jennifer received her a.b. in chemistry and religion from Dartmouth College in 1992.*

Jerry Tull *has been a Scientist at SciTec, Inc. since 1996. He obtained a Ph. D. in chemistry at Princeton Unversity, where his thesis focussed on the development of ultrafast laser pulse shaping techniques and their application to chemical dynamics. Since he has been at SciTec, he has been involved with the development of target detection algorithms for hyperspectral data sources, as well as the development of algorithms for characterization of atmospheric conditions from multispectral remote sensing data.*

Jim Lisowski *is a Senior Scientist at SciTec, Inc., and has been the principal analyst for exploitation of data collected with ARES since its earliest flights in the mid-1980's. In recent years his focus has been on the interpretation and exploitation of transient event signature data and analyzing the nature and impact of clouds and terrain on overhead infrared sensors. Today, ARES related efforts involve the analysis and exploitation of hyperspectral data collected by the M/LWIR SEBASS system. Mr. Lisowski received his Bachelor's degree in Physics from Rutgers College in 1985 and has been a member of the technical staff at SciTec since 1984.*

Capt. Todd Caldwell